Surface & Coatings Technology 394 (2020) 125813

Contents lists available at ScienceDirect

Surface & Coatings Technology

journal homepage: www.elsevier.com/locate/surfcoat

Formation of ordered anodic alumina nanofibers during aluminum anodizing in oxalic acid at high voltage and electrical power

K. Chernyakova[a], A. Ispas[b], R. Karpicz[a], G. Ecke[b], I. Vrublevsky[c,*], A. Bund[b]

[a] Center for Physical Science and Technology, Saulėtekio Ave. 3, LT-10257 Vilnius, Lithuania
[b] Technische Universität Ilmenau, Gustav-Kirchhoff Str. 6, 98693 Ilmenau, Germany
[c] Belarusian State University of Informatics and Radioelectronics, P. Brovka Str. 6, 220013 Minsk, Belarus

ARTICLE INFO

Keywords:
Anodic alumina nanofibers
Oxalic acid
Auger spectroscopy
Fluorescence
High voltage anodizing

ABSTRACT

In this study, we modified the synthesis modes of aluminum anodizing in an aqueous solution of oxalic acid and suggested quick, one-step and convenient method for porous alumina surface modification to increase largely its surface area. Anodic alumina nanofibers consisting of pure aluminum oxide were formed by high field anodizing with evolving of Joule heating of aluminum foil of 60 and 100 μm thickness in 0.3 M aqueous solution of oxalic acid. It was shown that nanofibers formed on the surface of the films for an anodizing voltage of 90 V and a power range of 13.5–31.5 W cm^{-2}. The thickness of the Al foil has proved to be responsible for the formation of the alumina nanofibers, which cannot be obtained in the same electrolyte and for similar current densities on 25 μm thick aluminum foil. We could show that during anodizing of 60 μm thick Al foil, regardless of anodic current density value, alumina nanofibers uniformly covered the entire surface of the films. However, during 100 μm Al foil anodizing, the pores were etched and the nanofibers partially dissolved and separated from the surface with increasing anodizing current density. Auger electron spectroscopy measurements showed that porous anodic alumina containing carbon impurities was obtained during anodizing of the 25 μm Al foil. Alternatively, the surface of the nanofibers formed on 60 and 100 μm Al foil consisted of pure alumina.

1. Introduction

Aluminum oxide as a chemically inert and thermally stable material with high dielectric constant and low magnetic conductivity is widely used in catalysis, in the production of optoelectronic devices, sensors and fire protection systems [1,2]. Synthesis of alumina nanofibers and nanotubes [3,4], as well as the study of their properties are of great interest, as in this case a surface with a large reactive area is formed, which makes the alumina nanofibers suitable for use as catalysts, catalyst supports and absorbents. In addition, alumina nanofibers are good absorbents for purifying water wastes from the heavy metal ions, such as mercury, cadmium, and lead [5,6].

Alumina nanofibers can be synthesized by various methods, including hydrothermal synthesis, sol-gel method, chemical etching of porous alumina films, long-term anodizing of aluminum in solutions of two- and tribasic acids, as well as in the process of re-anodizing of Al_2O_3/Al electrodes in acidic solutions with fluorine-containing additives [6–10]. One of the most commonly used methods is the etching of porous alumina films in acidic [11] or alkaline solutions [12,13], but this process is quite time consuming and the size and shape of the resulting nanofibers could be sometimes rather difficult to control [14]. In contrast to chemical etching, ultra-high density single nanometer-scale anodic alumina nanofibers of controllable shape and size consisting of an amorphous pure alumina were fabricated via anodizing in pyrophosphoric acid, but there was one disadvantage, namely, the whole process took 24 h or even more [15,16].

Oxalic acid was also used as electrolyte for obtaining alumina nanofibers by anodizing electrochemical procedure. Two step anodization process was reported to produce nanofibers of uniform length (3 μm) and diameter (70 nm) [17]. Besides the high electric field (40 V for 4 and 8 h in the first and second anodization steps, respectively), the mechanical stress was also proved to be important factor when growing the nanofibers [18]. In another study, alumina nanofibers having lengths from several hundred nanometers up to tens of micrometers were produced by consecutively decreasing the anodizing voltage from 80 to 20 V, keeping it at 20 V for 120 min and then increasing it back to 56.5 V for > 20 h [19]. A combination constant and pulse voltage was used to obtained alumina nanofibers in 0.5 M oxalic acid [20]. Shao et al. showed that the frequency of the pulse voltage is more important for tuning the number of nanofibers than the duty cycle or the total

* Corresponding author.
E-mail address: vrublevsky@bsuir.edu.by (I. Vrublevsky).

https://doi.org/10.1016/j.surfcoat.2020.125813
Received 19 January 2020; Received in revised form 9 March 2020; Accepted 17 April 2020
Available online 30 April 2020

time of the pulses [20].

A mechanism that describes the nanofiber formation was proposed in [15], showing that nanofibers grew at the triple points of the honeycomb structure. One more method of synthesizing anodic alumina nanofibers using anodizing in an aqueous solution of oxalic acid at high anodizing current densities (325 mA cm^{-2}) was suggested in [21]. In this study, at the first stage of the process, Al foil was treated in 0.06 M Na_2SO_4 solution at 4 V bias at room temperature for 3 h and then, at the second stage, several micrometer long nanofibers were formed after approximately 20 min. The effect of anodizing modes on the morphology of nanofibers, their properties, and the mechanism of their formation have not been also discussed in details. Anodizing of aluminum foil in oxalic acid solution is a simple way to obtain alumina nanofibers, since in this case the process and, consequently, the final product is easy to control by changing the modes of electrochemical synthesis, such as voltage, time, and temperature.

In this present work we aimed to study the peculiarities of the formation of alumina nanofibers obtained during the electrochemical oxidation of aluminum with evolving of Joule heating in an aqueous solution of oxalic acid at high current densities, and to determine the effect of anodizing modes on the morphology, composition, structural, and optical properties of nanofibers. In our previous studies [22,23], we showed that the Joule heating generated in the barrier layer of porous alumina affected the temperature of the electrolyte at the bottom of the pore, and, as a result, the rate of dissolution of the oxide and the morphology of the film surface was also influenced. It is impossible to determine the temperature at the bottom of the pores directly, but the amount of Joule heating released can be changed by varying the anodizing conditions, such as the anodizing current density (J_a), voltage (U_a), time (t_a) and electrolyte temperature (T_e). In our case only varying in J_a makes sense, as electrolyte temperature in the range of 5–40 °C does not affect the morphology of the oxalic acid anodic alumina films [23]. During anodizing at high current densities, the process starts from the corner of the sample and then spreads over the entire surface, so it is local and varying in t_a becomes senseless [24]. Regardless the value of J_a at steady-state of oxide growth U_a also stays constant and, therefore, does not influence the morphology of the films [25]. As it was shown before [26], the oxide thickness under the same conditions (J_a, t_a and T_e) was different for different thickness of the specimens, hence, the heat transfer rate also depends on thickness of the Al foil. So, both anodizing current density and Al foil thickness might affect the morphology and properties of anodic alumina films. Therefore, in order to estimate these effects, we prepared samples on Al foil with thickness of 25, 60 and 100 μm, then anodized them at various J_a values in the range from 150 to 350 mA cm^{-2}. This study is the first one, to the best of our knowledge, describing the effect of the thickness of the substrate on the properties of the formed alumina nanofibers.

2. Materials and methods

2.1. Anodizing

The samples were prepared on the high-purity aluminum foil (99.99%) of different thickness (25, 60 and 100 μm thick, 10 × 10 mm, Alfa Aesar). The aluminum specimens were pretreated in a hot solution of 1.5 M NaOH for 15 s, neutralized in 1.5 M HNO_3 for 2 min, then carefully rinsed in distilled water and air-dried. Anodic alumina was formed by double-sided anodizing of aluminum specimens in a 0.3 M aqueous solution of oxalic acid up to the moment when the aluminum was completely oxidized at the constant current mode. For each anodizing time did not exceed 15 min. The current density (J_a) was varied in the range of 150–350 mA cm^{-2} with the step of 50 mA cm^{-2}. At the steady state of oxide growth, the anodizing voltage (U_a) was of about 90 V (electrical power was about of 13.5–31.5 W cm^{-2}). The anodizing process was carried out in two-electrode glass cell, in which a platinum grid was used as counter electrode. The solution was mechanically stirred with a magnetic stirrer, and the temperature of the electrolyte was maintained at a constant value (15.0 ± 0.1) °C with a Haake K15 thermostat. The anodizing process was controlled by a direct current power supply GW Instek (GPR–30H100). If indicated, for fluorescence and SEM studies the samples were ultrasonically treated to remove alumina nanofibers from the surface of the substrate.

2.2. Characterization

Surface morphology of the films was analyzed by scanning electron microscopy (SEM) on a Hitachi S-4800 device. Subsequent statistical analyses of the images were performed by ImageJ software by a procedure previously described in [22,23]. The Auger electron spectroscopy (AES) measurements were performed to investigate the chemical states of the elements on the surface of oxalic acid alumina films using a Thermo VG Scientific Microlab 350 instrument, equipped with a concentric hemispherical analyzer. The electron beam current was 14.1 nA at a spot size of 30 nm and acceleration voltage 10 keV. Scanning was done on different regions of several square micrometers (10–300 μm^2) on the alumina samples, in a 0.8 eV step, between 30 and 1700 eV. The modulation amplitude of phase sensitive detector was set at 865 eV. Different detection angles have been used. The SEM images were taken at 0°, 30°, 40° and 60° tilt. The alumina films have insulating properties. Therefore, it was impossible to measure a reproducible spectrum if the incident electron beam was perpendicularly to the surface of the sample. The Auger signal was best when the samples of 100 μm were tilt at 40° and when the ones of 60 μm were tilt at 60°. The 25 μm alumina foils were more easily charged at low tilting angles under electron irradiation, therefore, for measuring these samples a tilt of 80° was used.

Fluorescence spectra were measured with a time-correlated single photon counting spectrometer Edinburgh-F900 (Edinburg instruments). A picosecond pulsed diode laser EPL-375 emitting picosecond (76 ps) duration pulses was used for the excitation at 375 nm with an average power 0.15 mW mm^{-2}. The pulse repetition rate was 5 MHz and the time resolution of the setup was about 100 ps considering temporal deconvolution procedure. All fluorescence spectra were corrected for the instrument sensitivity.

3. Results and discussion

3.1. Surface characterization

Anodizing of 25 μm Al foil at J_a = 150–350 mA cm^{-2} results in the formation of a disordered pore arrays on the surface of the films (Fig. 1a–c). At J_a = 150 mA cm^{-2} pore diameter (d_p) equals to 53 nm, and d_p remains almost the same with increasing anodizing current density to 250 mA cm^{-2}, but at J_a = 300–350 mA cm^{-2} d_p significantly reduces to 40 nm (Fig. 2). Our results are in good agreement with d_p values reported by Lee et al. [27] for the processes of hard aluminum anodizing in a 0.3 M aqueous solution of oxalic acid at anodizing potentials, U_a, between 100 and 160 V and $J_a \geq 250$ mA cm^{-2}. It should be noted here that no nanofibers were formed during 25 μm Al foil anodizing, independent on the J_a value applied. At the same time, nanofibers were obtained on the surface of the 60 and 100 μm Al foil (Fig. 1d–i). They originate at the triple junction points and collapse one another to form a mesh structure above pores (Fig. 3).

It can be seen in Fig. 1d–f, that the anodizing current density affects drastically the process of nanowire formation in the case that 60 μm and 100 μm Al foil was used. The surface still remains porous for alumina produced on 60 μm Al film at J_a = 150 mA cm^{-2}, but the pore walls dissolve and the beginning of the formation of alumina nanofibers is observed. Nanofibers are formed over the entire surface of the films starting from J_a = 200 cm^{-2}. In the case of the 100 μm Al foil, the sample is not completely covered with nanofibers after anodizing. It can be seen that some nanofibers are partially dissolved and peeled off from

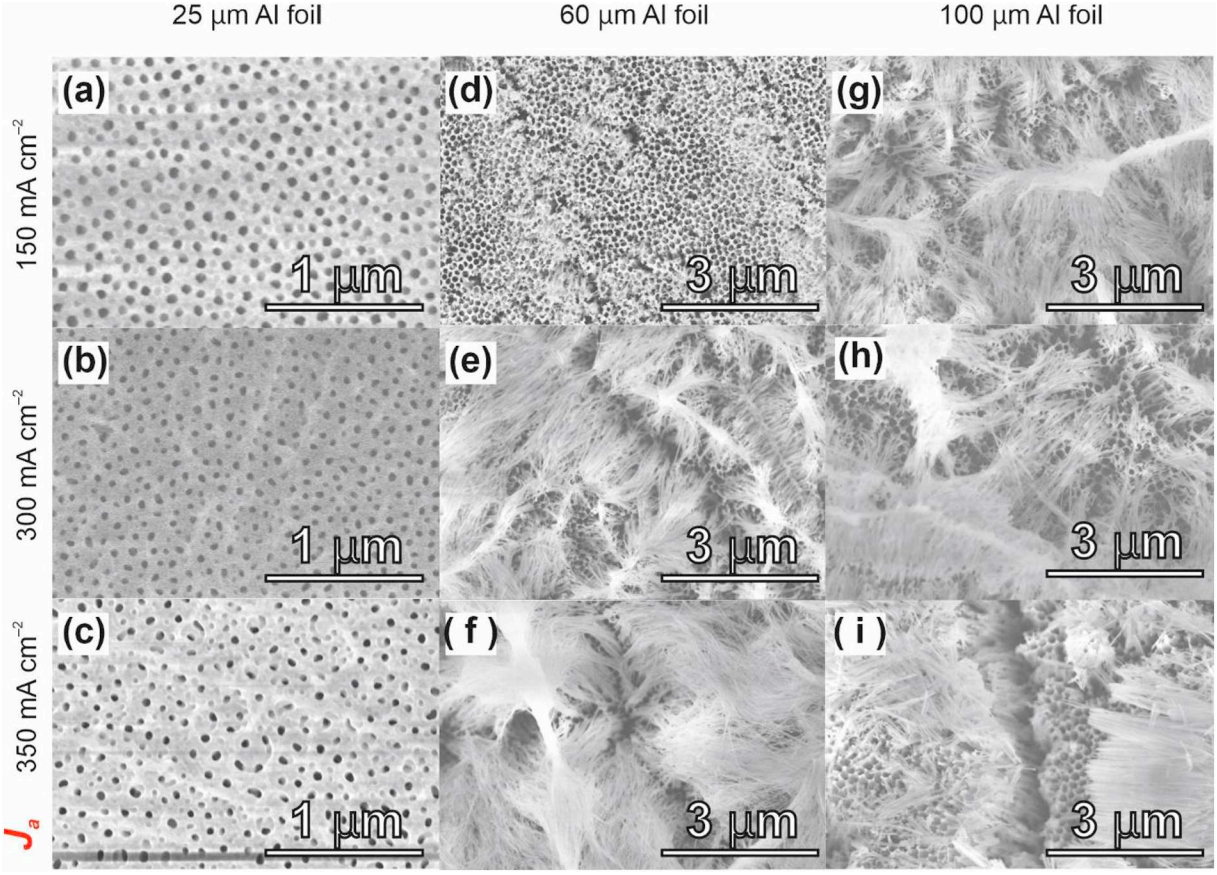

Fig. 1. SEM images of the top surface of oxalic acid anodic alumina films formed on 25 μm (a–c), 60 μm (d–f) and 100 μm (g–i) Al foil at different anodizing current, as indicated on the left-hand side of the images.

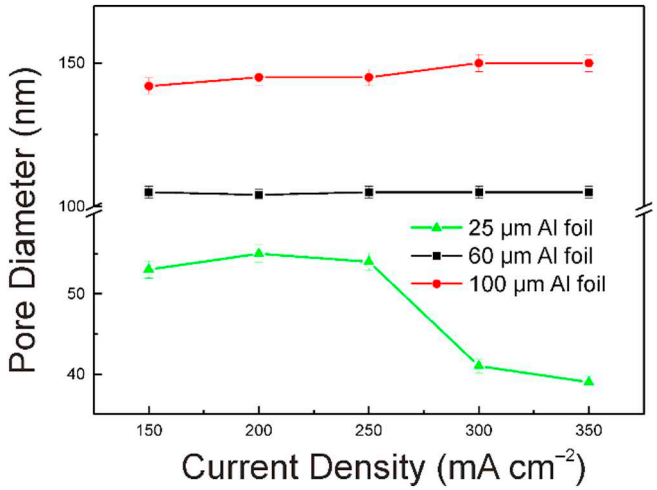

Fig. 2. Variations in pore diameter of oxalic acid anodic alumina films formed on 25, 60 and 100 μm Al foil as a function of anodizing current. For 60 and 100 μm Al foil, the porous structure below nanofibers was considered in calculation.

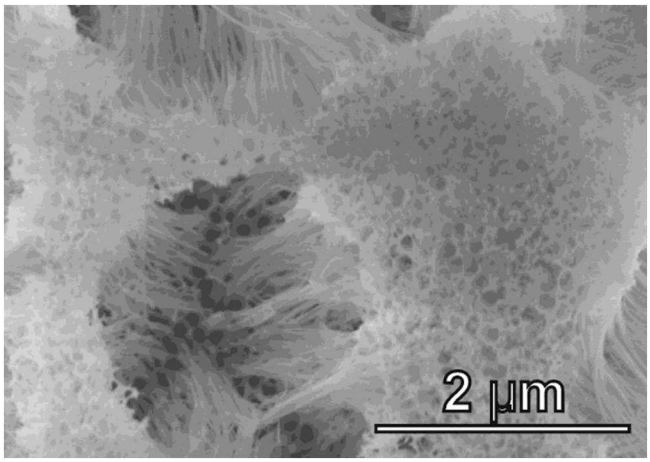

Fig. 3. Alumina nanofibers originating at the triple junctions of the pores and then collapsing onto one another to form a mesh structure above the surface. The films were formed on 60 μm Al foil at 250 mA cm^{-2}.

the porous surface, and this effect is enhanced with increasing the J_a (Fig. 1g–i).

To determine the effect of J_a on the porous structure of the films, we investigated the oxide surface below the nanofibers (Figs. 2 and 4). In the case of 60 μm Al foil, d_p is ca. 105 nm regardless of the J_a value. For 100 μm Al foil, d_p increases from 142 to 150 nm with increasing anodizing current, and at the same time highly ordered porous structure is formed. As it can be seen from Fig. 5, interpore distance (D_{int}) is practically independent of the J_a, and is only a function of the thickness of Al foil. For 25, 60 and 100 μm foil D_{int} is equal to 132–135 nm, 148–152 nm and 197–200 nm, respectively. For 100 μm Al foil D_{int} values coincide with those given in the literature [27]. However, for the samples obtained on 25 and 60 μm foil D_{int} values are less by 33 and 25%, respectively. This can be explained by the fact that in the previous studies the Al foil with thickness of 250 μm was used [21], therefore, during 25 and 60 μm Al foil anodizing, the foil thickness was not enough to form the cells of normal size. In addition, the dependence of D_{int} on the anodizing current density is somewhat different from the

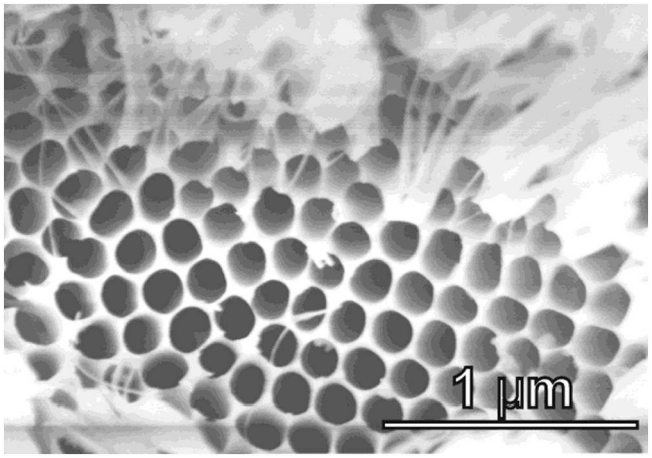

Fig. 4. Pore structure below the nanofibers for oxalic acid anodic alumina formed on 100 μm Al foil at J_a = 200 mA cm^{-2}.

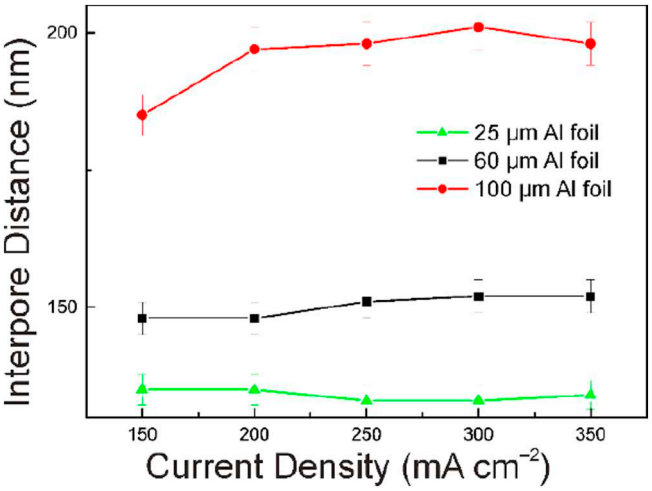

Fig. 5. Variations in interpore distance of oxalic acid anodic alumina films formed on 25, 60 and 100 μm Al foil as a function of anodizing current. For 60 and 100 μm Al foil, the porous structure below nanofibers was considered in calculation.

previously described [27–29]. During experiments at constant voltage mode (maximal J_a value was about 1000 mA cm^{-2}) it was established that J_a was a key parameter affecting D_{int}, i.e. with increasing J_a, D_{int} should decrease [27,28,30]. At the same time, it was shown that during constant current anodizing, J_a = 75 mA cm^{-2}, D_{int} was directly proportional to the U_a on steady state of oxide growth. Thus, in our experiments, the independence of D_{int} from J_a can be explained by the small difference between the minimum and maximum values of J_a (ΔJ_a = 200 mA cm^{-2}) compared to ΔJ_a = 750 mA cm^{-2} used in [27,28], and by the fact that the value of U_a was constant and did not depend on the density of the anodizing current at the steady state of oxide growth.

Therefore, during anodizing of Al foil with a thickness of 60 μm, regardless of J_a value, alumina nanofibers uniformly cover the entire surface of the films, the pore diameter under the wires also remains almost unchanged, which is the evidence of the stable process of nanowire growth. Alternatively, during anodizing of 100 μm Al foil the pores are etched and the nanofibers partially dissolve and separate from the surface with increasing J_a, and this process continues until the end of anodizing. Obviously, with increasing Al foil thickness, the anodizing time increases as does the thickness of the formed alumina, which leads to a decrease in thermal conductivity of thicker samples and also to the local overheating in the barrier layer, i.e. in films obtained on 60 and 100 μm Al foil, Joule heating dissipates worse than in the case of 25 μm foil. As a result, the local temperature at the bottom of the pores increases, electrolyte heats up and, therefore, the rate of dissolution of the outer (containing electrolyte ions or products of their oxidation) oxide layer increases. Since nanofibers are formed at the junction of three hexagonal cells and consist of pure alumina [15,16], the impure pore walls dissolve faster than the pure oxide, which contributes to the formation of nanofibers. The same process took place during nanowire formation during etching of porous alumina in alkaline solutions [6,8].

3.2. Structural characterization

As it was mentioned above the surface of the anodic alumina obtained on 25 μm Al foil was porous, therefore, according to the general theory of the structure of the porous anodic alumina pore walls must contain electrolyte species [31], in our case besides aluminum and oxygen carbon must be also present. However, nanofibers are pure alumina, therefore, on the surface of the fibrous samples carbon should be absent [15,16]. To establish the effect of anodizing modes on the composition of alumina nanofibers the surface of the anodic alumina films obtained at different modes was studied by AES. Three lines with maxima at ca. 470, 485 and 503 eV were observed in the Auger spectra of all samples (Fig. 6), in the kinetic energy (KE) range of 465–504 eV, corresponding to KL_1L_1, KL_1L_{23} and $KL_{23}L_{23}$ transitions in the Auger spectrum of oxygen [32,33]. There are also lines in the KE 1300–1400 eV region, corresponding to *KLL* transitions in the spectrum of aluminum. The line with maximum intensity has KE at ca. 1385 eV and corresponds to the $KL_{23}L_{23}$ transition of the Al^{3+} ion in alumina [34–37]. In addition to the main lines of oxygen and aluminum, in the spectra of the films obtained on 25 μm Al foil there is a carbon line with KE at ca. 270 eV ($KL_{23}L_{23}$ carbon transition, [38]), which is absent in the spectra of samples formed on 60 and 100 μm foil. Nanofibers consist of pure alumina in this case [15,16], and no carbon lines were observed in Auger spectra. However, there are no nanofibers on the surface of thin films (25 μm), consequently, the oxide layer contains products from the oxidation of oxalate ions, which are clearly seen in the Auger spectra (Fig. 1a–c). This agrees with previous studies on composition of porous alumina films [39,40].

It should be noted that the Auger spectra of samples obtained on a foil of the same thickness, but at different J_a, practically do not differ from each other. At the same time, the O *KLL* spectra turned out to be sensitive to the surface structure of anodic alumina films, i.e. when pores were changed to nanofibers (Figs. 1 and 6). The Auger spectrum of a porous alumina formed on a 25 μm Al foil completely coincides with the standard aluminum oxide spectrum given as reference in text books [41]. However, in the spectra of samples obtained on a thicker foil, both the oxygen lines and the aluminum lines are less resolved; moreover, their overall intensity and intensity of the individual lines relative to each other also differ significantly from the reference ones. In our case in the spectrum of O *KLL*, the intensities of O $KL_{23}L_{23}$ and O KL_1L_1 transitions are almost the same, which is rather unusual.

According to [42,43], O *KLL* emission involves two valence electrons from O 2*s* (L_1), O $2p_{1/2}$ (L_2) or O $2p_{3/2}$ (L_3), therefore, it is sensitive to the oxidation state (effective charge) of the oxygen atoms. However, it is rather difficult to obtain quantitative information about the effective charge from these spectra, because Auger excitation is a complex process, but a qualitative analysis can be performed. It is assumed that the formation of bonds between the oxygen atom and neighboring atoms occurs mainly due to the O 2*p* orbitals rather than the O 2*s* level. As a result, the intensity of the O *KLL* lines, in which electrons from the L_2 and L_3 levels are involved, should be more sensitive to changes in the valence state of oxygen atoms than the Auger transitions involving L_1 orbital. Consequently, a high valence charge at L_2 and L_3 levels corresponds to a higher probability of O $KL_{23}L_{23}$ transition, at the same time, the probability of O KL_1L_1 transition should be less dependent on changes in the valence charge, i.e. in the O

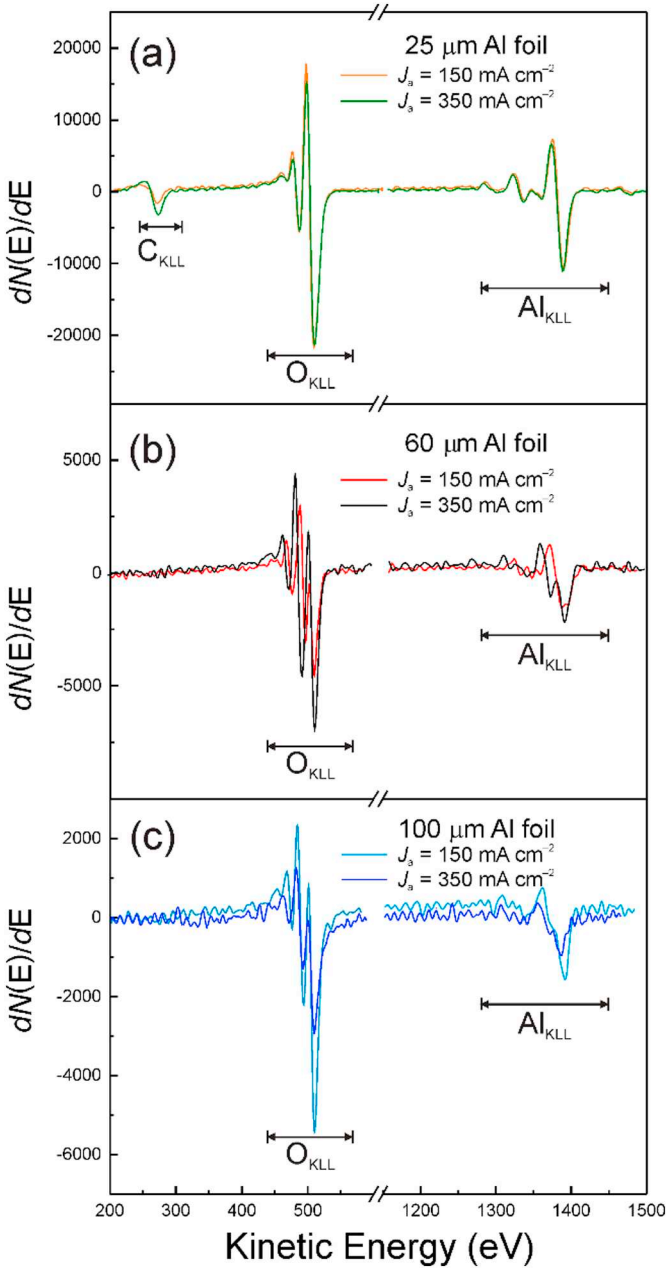

Fig. 6. Auger spectra of oxalic acid anodic alumina films formed on 25 μm (a), 60 μm (b) and 100 μm (c) Al foil at different anodizing current.

KLL spectrum the intensity ratio of O $KL_{23}L_{23}$ and O KL_1L_1 lines (I_3/I_1) is a measure of the of oxygen oxidation state. In [44] for different oxides, the empirical dependencies of I_3/I_1 have been also established. Using them one can evaluate the effective charge on oxygen atom, namely, it was shown that the larger value of I_3/I_1 could correspond to the lower effective charge on the oxygen atom. This conclusion suggests oxygen deficiency in the alumina nanofibers formed on the surface of anodic alumina. However, this is not a valid explanation in our case, because, as described in [45], at triple junction points alumina of stoichiometric composition forms and nanofibers grow directly from these points. Therefore, changes in the shape of O *KLL* and Al *KLL* Auger spectra probably result from the nanostructured fibrous surface of the samples, but not from the formation of oxygen defective alumina.

Fluorescence spectroscopy is an experimental method for the determination of various defects, so we registered the steady state and time resolved fluorescence spectra of the samples obtained on 100 μm

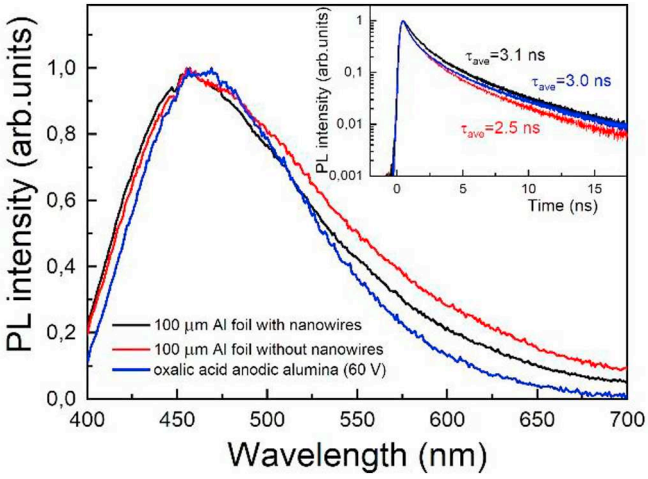

Fig. 7. Steady-state fluorescence spectra of the oxalic acid anodic films formed on 100 μm Al foil at J_a = 350 mA cm^{-2} with alumina nanofibers on the surface (black curve), without nanofibers (red curve) and film formed at 60 V (blue curve), λ_{ex} = 375 nm. All spectra were normalized to maximum intensity. Inset shows fluorescence decay kinetics of the oxalic acid alumina films. (For interpretation of the references to color in this figure legend, the reader is referred to the web version of this article.)

Al foil, with and without nanofibers on the surface, and anodic alumina formed in oxalic acid solution at 60 V (Fig. 7). This sample was chosen as a reference, because the composition and fluorescent properties of anodic alumina obtained in oxalic acid solution are well studied [46]. The steady state fluorescence spectra (λ_{ex} = 375 nm) of all films are characterized by a wide band in the wavelength range of 400–700 nm with a maximum of emission band at 460 nm. For a better qualitative comparison, the spectra were normalized to a maximum of intensity. For films with nanofibers on the surface and alumina films obtained at 60 V, the full width at half maximum is 120 and 110 nm, respectively. According to time resolved fluorescence data the average lifetime of the luminescence centers (τ_{ave}) for these films is almost the same, and equals to ca. 3.0 ns. The spectrum for the sample without nanofibers on the surface broadens, the full width at half maximum is 135 nm, and τ_{ave} decreases to 2.5 ns (Fig. 7, inset). Spectrum characteristics become similar to those of carbon-bearing anodic alumina obtained in tartaric acid solution [25,27]. According to [25,42] the broadening of the spectrum and the decrease in τ_{ave} is associated with the formation of amorphous carbon in the process of anodizing aluminum in solutions of organic acids at high current densities. Consequently, on the surface of nanofibers, the nature and number of defects do not significantly differ from those for the reference sample. Moreover, it can be argued that the unusual shape of Auger spectra of nanofibers is associated precisely with their fibrous nanostructure.

4. Conclusions

It was established that aluminum substrate thickness affected the morphology of the films obtained, i.e., alumina nanofibers were obtained on the surface of the 60 and 100 μm Al foil, but at the same time, they were not formed during anodizing in a 0.3 M aqueous solution of oxalic acid of 25 μm Al foil, independent on the J_a value used. It was shown that among the substrate thicknesses (25, 60 and 100 μm) and anodizing currents (150–350 mA cm^{-1}) used in the investigation, alumina nanofibers uniformly covered the entire surface of the films formed only on the Al foil with a thickness of 60 μm at J_a high then 200 mA cm^{-2}. It was remarkable that, the pore diameter under the wires also remained almost unchanged, which indicated the stable process of alumina nanofibers growth. However, during 100 μm Al foil anodizing, the pores were etched and the nanofibers partially dissolved

and separated from the surface with increasing anodizing current density, and this process continued until the end of anodizing.

By Auger spectroscopy it was established that porous anodic alumina containing carbon impurities was obtained during 25 μm Al foil. Alternatively, the surface of the samples formed on 60 and 100 μm Al foil did not contain carbon and consisted only of pure alumina. In addition, for these samples, in Auger spectra both the oxygen line and the aluminum line were worse resolved, and their overall intensity and intensity of individual lines relative to each other were also different from the reference. Analysis of Auger and fluorescent data allowed us to conclude that changes in the shape of O *KLL* and Al *KLL* were associated with their fibrous nanostructure.

CRediT authorship contribution statement

K. Chernyakova: Supervision, Conceptualization, Investigation, Writing - original draft, Validation, Formal analysis.**A. Ispas:**Investigation, Data curation, Writing - original draft, Validation.**R. Karpicz:**Investigation, Visualization, Writing - review & editing.**G. Ecke:**Investigation, Visualization.**I. Vrublevsky:** Conceptualization, Methodology, Formal analysis, Software, Validation, Visualization, Writing - review & editing.**A. Bund:**Conceptualization, Methodology, Validation, Project administration.

Declaration of competing interest

The authors declare that they have no known competing financial interests or personal relationships that could have appeared to influence the work reported in this paper.

Acknowledgements

R.K acknowledges a partly funding from the Research Council of Lithuania under project no. S-LB-19-4.

References

[1] J. Xu, A. Wang, X. Wang, D. Su, T. Zhang, Nano Res. 4 (2011) 50–60.
[2] S.E. Kushnir, K.S. Napolskii, Mater. Des. 144 (2018) 140–150.
[3] S. Song, H. Oh, H. Kong, J. Jang, J. Hazard. Mater. 187 (2011) 311–317.
[4] J. Zou, L. Pu, X. Bao, D. Feng, Appl. Phys. Lett. 80 (2002) 1079–1081.
[5] S. Thavamani, R. Rajkumar, Res. J. Chem. Sci. 3 (2013) 44–48.
[6] T. Kikuchi, K. Kunimoto, H. Ikeda, D. Nakajima, R.O. Suzuki, Sh. Natsui, J. Electroanalyt. Chem. 846 (2019) 113152.
[7] Y.T. Tian, G.W. Meng, T. Gao, S.H. Sun, T. Xie, X.S. Peng, C.H. Ye, L.D. Zhang, Nanotechnology 15 (2004) 189–191.
[8] X.X. Sun, J. Liang, J.F. Zhao, Q. Ma, B.S. Xu, Appl. Phys. A Mater. Sci. Process. 98 (2010) 263–267.
[9] P.Y. Deng, X. De Baiz, X.W. Chen, Q.L. Feng, J. Electrochem. Soc. 151 (2004) B284–B289.
[10] A. Jagminas, J. Kuzmarskyte, L. Malferrari, M. Cuffiani, Mater. Lett. 61 (2007) 2896–2899.
[11] Y.F. Meia, G.G. Siu, R.K.Y. Fu, P. Chen, X.L. Wu, T.F. Hung, P.K. Chu, J. Appl. Phys. 97 (97) (2005) 034305.
[12] Z.L. Xiao, C.Y. Han, U. Welp, H.H. Wang, W.K. Kwok, G.A. Willing, J.M. Hiller, R.E. Cook, D.J. Miller, G.W. Crabtree, Nano Lett. 2 (2002) 1293–1297.
[13] J. Kim, Y.C. Choi, K.-S. Chang, S.D. Bu, Nanotechnology 17 (17) (2006) 355–359.
[14] L. Zhang, B. Cheng, W. Shi, E.T. Samulski, J. Mater. Chem. 15 (2005) 4889–4893.
[15] T. Kikuchi, O. Nishinaga, D. Nakajima, J. Kawashima, Sh. Natsui, N. Sakaguchi, R.O. Suzuki, Sci. Rep. 4 (2014) 7411.
[16] D. Nakajima, T. Kikuchi, Sh. Natsui, N. Sakaguchi, R.O. Suzuki, Appl. Surf. Sci. 356 (2015) 54–62.
[17] M.R. Kim, J.Y. Kim, D.-J. Jang, Eur. Phys. J. D 43 (2007) 279–282.
[18] K.G. Zhu, J.R. Cheng, M.C. Chang, W. Wang, W.B. Wie, G.L. Ge, Chin. Sci. Bull. 56 (2011) 1947–1955.
[19] Z.H. Su, X.C. Li, F.M. Qu, H.J. Zhou, L. Liu, Q. Zhou, L. Zhang, H. Wang, M. Feng, Y.F. Wang, X.W. Cao, Solid State Commun. 149 (2009) 1782–1785.
[20] X.F. Shao, X.L. Wu, G.S. Huang, T. Qiu, M. Jiang, J.M. Hong, Appl. Phys. A Mater. Sci. Process. 81 (2005) 621–625.
[21] W. Wu, X. Wang, D. Wang, M. Chen, F. Zhou, W. Liu, Q. Xue, Chem. Commun. (2009) 1043–1045.
[22] I. Vrublevsky, A. Ispas, K. Chernyakova, A. Bund, J. Solid State Electrochem. 20 (2016) 2765–2773.
[23] K. Chernyakova, I. Vrublevsky, V. Klimas, A. Jagminas, J. Electrochem. Soc. 165 (2018) E289–E293.
[24] A. Jagminas, G. Grincienė, A. Selskis, K. Chernyakova, Phys. Chem. Chem. Phys. 21 (2019) 14941–14944.
[25] K.V. Chernyakova, R. Karpicz, S. Zavadski, O. Poklonskaya, A. Jagminas, I. Vrublevsky, J. Lumin. 182 (2017) 233–239.
[26] Th. Skoulikidis, Ath. Karageorgos, M. Nersisyan, Proc. of the 6th Int. Congress on Marine Corr. and Fouling, (1984), pp. 41–46.
[27] W. Lee, R. Ji, U. Goesele, K. Nielsch, Nature Mater 5 (2006) 741–747.
[28] K. Schwirn, W. Lee, R. Hillebrand, M. Steinhart, K. Nielsch, U. Goesele, ASC Nano 2 (2008) 302–310.
[29] Y. Song, L. Jiang, W. Qi, C. Lu, X. Zhu, H. Jia, J. Electroanal. Chem. 673 (2012) 24–31.
[30] M. Ghorbani, F. Nasirpouri, A. Iraji zad, A. Saedi, Mater Des. 27 (2006) 983–988.
[31] G.D. Sulka, Ch. 1 (Highly Ordered Anodic Porous Alumina Formation by Self-organized Anodizing) in Nanostructured Materials in Electrochemistry pp. 1–116, Wiley-VCH Verlag GmbH & Co. KgaA, Ed.by Ali Eftekhari, (2008).
[32] J.C. Fuggle, E. Umbach, R. Kakoschke, D. Menzel, J. Electron Spect. Rel. Phenom. 26 (1982) 111–132.
[33] A. Hoffman, Ts. Maniv, M. Folman, Surf. Sci. 182 (1987) 56–68.
[34] G. Dufour, J.-M. Mriot, P.-E. Nilsson-Jatko, R.C. Karnatak, Phys. Scr. 13 (1976) 370–372.
[35] C.E. Moffitt, B. Chen, D.M. Wieliczka, M.B. Kruger, Solid State Comm. 116 (2000) 631–636.
[36] B. Timmermans, N. Vaeck, A. Hubin, F. Reniers, Surf. Interface Anal. 34 (2002) 356–359.
[37] M. Huttula, L. Partanen, A. Mäkinen, T. Kanita, H. Aksela, S. Aksela, Phys. Rev. A 79 (2009) 023412-1–023412-6.
[38] T.S. Sun, D.K. McNamara, J.S. Ahearn, J.M. Chen, B. Ditchek, J.D. Venables, Appl. Surf. Sci. 5 (1980) 406–425.
[39] Y. Xu, G.E. Thompson, G.C. Wood, B. Bethune, Corr. Sci. 27 (1987) 83–102.
[40] V.P. Parkhutik, Corr. Sci. 26 (1986) 295–310.
[41] L.E. Davis (Ed.), Handbook of Auger Electron Spectroscopy. A Reference Book of Standard Data for Identification and Interpretation of Auger Electron Spectroscopy Data, 2nd ed, Physical Electronics Industries, Inc., 1976(143 p).
[42] R. Weissmann, Solid State Comm. 31 (1979) 347–349.
[43] O. Boese, W.E.S. Unger, E. Kemnitz, S.L.M. Schroeder, Phys. Chem. Chem. Phys. 4 (2002) 2824–2832.
[44] C.D. Wagner, D.A. Zatko, R.H. Raymond, Anal. Chem. 52 (1980) 1445–1451.
[45] F. Le Coz, L. Arurault, L. Datas, Mater. Charact. 61 (2010) 283–288.
[46] S. Stojadinovic, R. Vasilic, Curr. Nanosci. 11 (2015) 547–559.